Using hyperspectral unmixing for the analysis of very high spatial resolution hyperspectral imagery

Ana C. Chavez Lopez[1], Manuel M. Goez Mora[2], Maria C. Torres-Madroñero[2], Miguel Velez-Reyes[1] [1]Sensor and Signal Analytics Laboratory, Electrical and Computer Engineering
[1]The University of Texas at El Paso, El Paso, Texas, USA
[2]Instituto Tecnológico Metropolitano, Medellín, Colombia

ABSTRACT

Traditional hyperspectral unmixing is focused on subpixel material composition extraction for low and moderate resolution imagery. Technological advances are making affordable hyperspectral imagers that can be used for very high spatial resolution imaging in many applications. A question that we want to address in this work is whether a traditional hyperspectral image analysis technique like unmixing still has value in the context of very high spatial resolution hyperspectral imaging (VHSR-HSI). In this paper, we will present preliminary results on how unsupervised hyperspectral unmixing algorithms can be used to extract spectral signatures of materials in a VHSR-HSI to map their spatial distribution and capture their spectral variability. Examples using hyperspectral images collected at close range using a standoff hyperspectral imager and an unmanned airborne system are used to illustrate our approach.

Keywords: hyperspectral imaging, unmixing, very high spatial resolution imaging, unsupervised unmixing, endmember extraction

1. INTRODUCTION

Unmixing is a valuable analysis technique to analyze satellite and airborne hyperspectral imagery of low to moderate spatial resolution. As imagers become more affordable, very high spatial resolution hyperspectral imaging is used in laboratory, computer vision, standoff, close-range and UxS remote sensing applications [1, 2, 3]. An interesting question we are trying to address in this work is if hyperspectral image processing techniques designed for moderate to low-resolution imagery can still be of value in very high spatial resolution hyperspectral imaging (VHSR-HSI).

In traditional HSI analysis, the linear mixing model assumes that the measured pixel spectral signature is the linear convex combination of the spectral signatures of the endmember signatures. However, in close-range imaging, the spatial resolution may be in the centimeter range, which will result in purer pixels across the scene so one could question why to use unmixing analysis in such an application. In this paper, we study the use of unmixing techniques to extract the spectral signatures present in the image and their spatial distribution. We also study the use of a simple variation of the Pixel Purity Index (PPI) endmember extraction algorithm where pixel votes are counted for maximum or minimum occurrences rather than just maximum like in traditional PPI and the criteria on selecting the number of endmember is by selecting the pixels that receive the top 2% of the votes. Clustering is then used to group similar endmember signatures and extract endmember classes that capture the spectral variability of a particular material signature. Abundance maps are obtained for each endmember class to obtain the spatial distribution of the material.

We study the use of unmixing with very high-resolution hyperspectral images collected of a vegetation plot from the International Tundra Experiment (ITEX) - Arctic Observatory Network (AON) in Utqiaġvik (formerly Barrow), Alaska and from Avocados fields in Antioquia, Colombia using a dual HySpex Mjolnir VS-620 hyperspectral imager on board of a drone.

2. METHODS

2.1 Hyperspectral Unmixing

Hyperspectral remote sensing involves capturing spectral data from many contiguous high spectral resolution bands across the electromagnetic spectrum, resulting in a spectral signature for each pixel in an image. The spectral signature of a pixel is a mixture of the spectral signatures of the various materials present in the instantaneous field of view of the sensor. The linear mixture model represents the measured signature as a linear convex combination of the spectral signature of the materials present in the sensor's field of view.

The linear unmixing aims to extract from the measured mixed spectral signature the number of endmembers, their spectral signatures, and their abundances or fractional area coverage within each pixel of the given hyperspectral image. By identifying the endmembers and their abundances, unmixing enables the identification and mapping of different materials within a scene, which is useful for numerous remote sensing applications. Various techniques have been proposed in the literature to address the unmixing problem [4, 5, 6].

Traditional methods for unmixing involve a two-step approach where first endmembers are determined and second, abundances are computed. In this work, a modified version of the pixel purity index (PPI) endmember extraction approach is used for endmember extraction. PPI generates random vectors or skewers in the spectral space (or feature space depending on the implementation) [7, 8]. Each pixel in the hyperspectral image is projected onto the random vectors and the number of times a particular pixel is selected as a maximum or minimum value in the process is recorded. Pixel signatures with high number of votes are considered candidates for endmember.

Once endmembers are available, the next step in unmixing is abundance estimation. Let

$$= [\ _{I} \quad \ldots \quad _{I}]$$

be the matrix of endmembers where $_{I}$ is the matrix containing the signatures of the spectral endmembers belonging to the i-th endmember class. The abundances for individual spectral endmembers is computed by solving a fully constrained linear least squares problem:

$$\mathrm{I} = \arg\min_{\mathrm{I}\,\mathrm{nI}_{\mathrm{II}}} \| - \quad \|$$

where is the pixel spectral signatures, and is the vector of spectral endmember abundances. Abundances are constrained to be positive and sum to one for a pixel. The abundances for an individual endmember class $_{I}$ is the sum of the abundances of the individual spectral endmembers. Multiple algorithms are available to solve this problem, see [9] as an example.

2.2 Data

Two VHSR-HSI data sets were used in this analysis. True color composites for these images are shown in Figure 1. The first image is from an ITEX-AON plot collected in Utqiaġvik (formerly Barrow) in summer of 2017. This image was collected using a SOC710-VP stand off hyperspectral imager from Surface Optics Corporation. The image is 696 lines by 520 samples, and 128 bands at 4.96 nm spectral resolution ranging from 375.25 nm to at 1038.25 nm. The second image is a UAV image from the Avocado trail in La Selva Research Center of the Colombian Agricultural Research Corporation (AGROSAVIA) in Rionegro, Antioquia, Colombia. The site is at 2093 meters above sea level. The region experiences an average annual temperature of 17°C, precipitation of 1917 mm, and relative humidity of 78%. The study was conducted in the Low Montane Humid Forest (bh-MB) ecological life zone, in the Rionegro Association cartographic unit, on a low alluvial terrace of the Rionegro River. The plants were studied over 19 months with wet soil conditions. The image was collected using a Dual HySpex Mjolnir VS-620, which combines a HySpex Mjolnir V-1240 (400-1000 nm, 200 bands at 3.0nm resolution) and HySpex Mjolnir S-620 (970-2500 nm with 300 bands at 5.1nm resolution) into a common housing. A portion of the full scene used is here and is comprised of 181 lines, 146 samples and 360 bands and. Table 1 summarized the information related to each image.

Table 1: Hyperspectral images: Details from ITEX vegetation and Avocados images.

Characteristics	ITEX vegetation	Avocados image
Sensor(s) used	SOC710-VP	Dual HySpex Mjolnir VS-620
Image Size	696 lines, 520 samples, 128 bands	181 lines, 146 samples, 360 bands
Wavelength range	375.25 – 1038.25 nm	400 – 2500 nm
Spectral resolution	4.96 nm	5.1 nm
Location	Alaska, US	Antioquia, Colombia
Collection date	Summer, 2017	November, 2021

(a) (b)

Figure 1: Color composites: (a) ITEX plot and (b) Avocados image.

3. EXPERIMENTAL RESULTS

3.1 Unmixing Results

We used 10,000 projections in our PPI implementation. Figure 2 (a) and (b) present the PPI votes histogram for the ITEX plot and the Avocados images respectively. The vertical scale presents the number of pixels and the horizontal scale the number of votes received. The vertical scale is capped at 10 pixels in the plots shown in Figure 2 (a) and (b), as most pixels in the image receive no votes or very few votes and we wanted to highlight those that actually received votes. Figure 2 (c) and (d) show binary images highlighting pixels that received any votes during the process. Only 1133 pixels out of 362k pixels in the ITEX plot image received any votes and 949 out of 26k pixels for the Avocados image.

Spectral endmembers were selected by choosing those signatures that have a number of votes above a threshold. A threshold of 130 votes was selected for the ITEX plot and 165 votes for the Avocados image. These thresholds were selected by trial and error. Developing a more systematic approach is part of future work. Using these thresholds resulted in 17 spectral endmembers for the ITEX plot image and 20 for the Avocados image. Since many of the extracted spectral endmembers were very similar, k-means clustering using the Euclidean distance was used to group extracted signatures into endmember classes. The number of endmember classes (clusters) was selected manually. Clustering spectral endmembers enabled us group similar to endmembers together, capturing endmember spectral variability, and facilitating analysis and interpretation. The endmember classes spectral signatures and abundance maps are shown in Figure 3: Endmember classes

and abundances for ITEX plot image. Figure 3 for the ITEX plot and Figure 4 for the Avocados image. People working in those areas gave the labels for the endmember classes after analyzing the abundance maps.

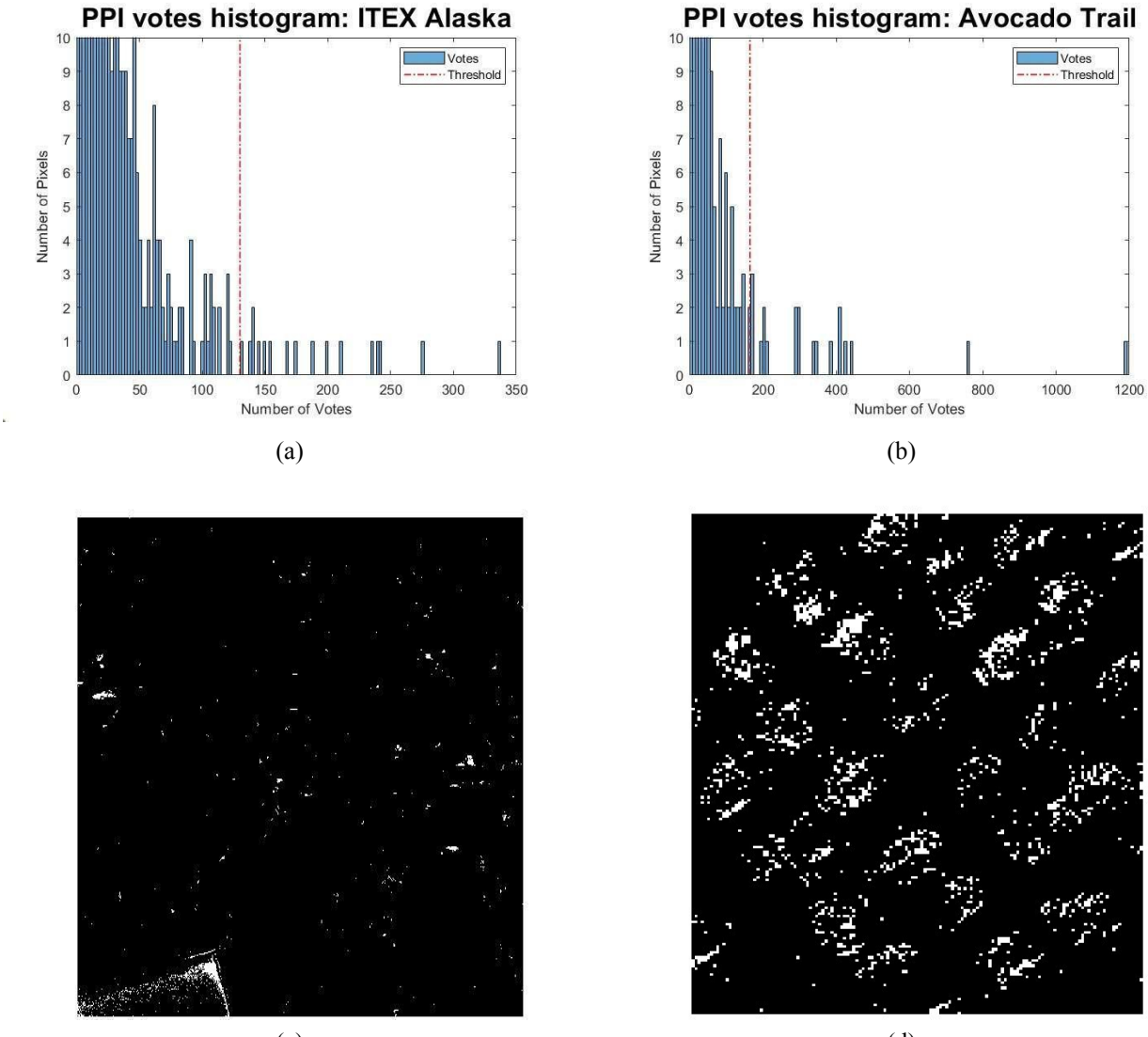

Figure 2. PPI results: (a) histogram for ITEX plot, (b) histogram for the Avocados image, binary map of pixel receiving at least one vote (c) ITEX plot, (d) Avocados image.

Color fractional maps [10] (RGB composites using abundance maps) are used to visualize spatial distribution and mixtures of endmember classes. The color fractional map for the ITEX plot is show in Figure 5(a). The fractional map was constructed by input the abundance for Cassiope Tetragona in the Green channel, and the abundance maps for Lichen Mixture 1 and 2 in the Red and Blue channels respectively. For the Avocados image (see Figure 5(b)), the color fractional map was generated by combining the abundances for Artifact 1 and 2 and used as input to the Red channel, Avocado plants to the Green channel, and Brighter avocado leaves to the Blue channel.

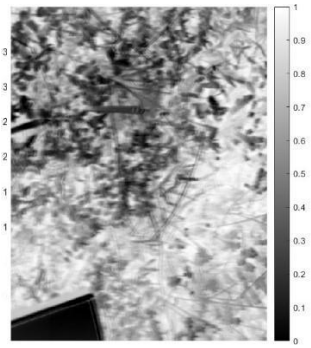

Lichen Mixture 1

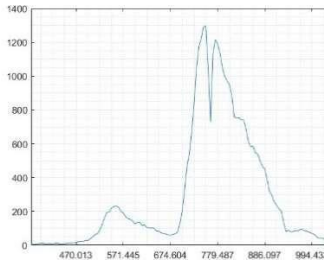

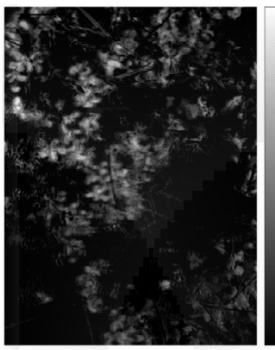

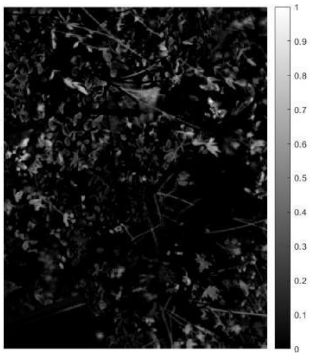

Lichen Mixture 2

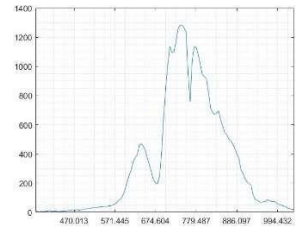

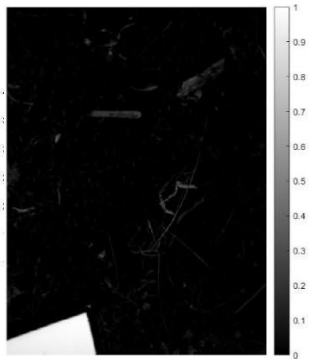

Wood Frame

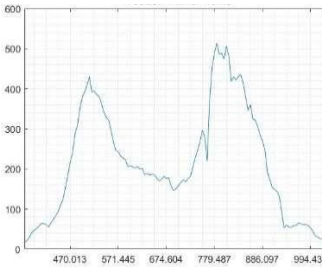

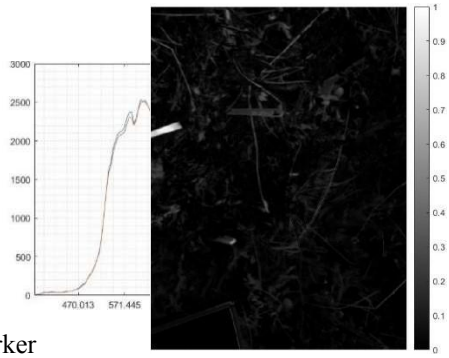

Wood Marker

Figure 3: Endmember classes and abundances for ITEX plot image.

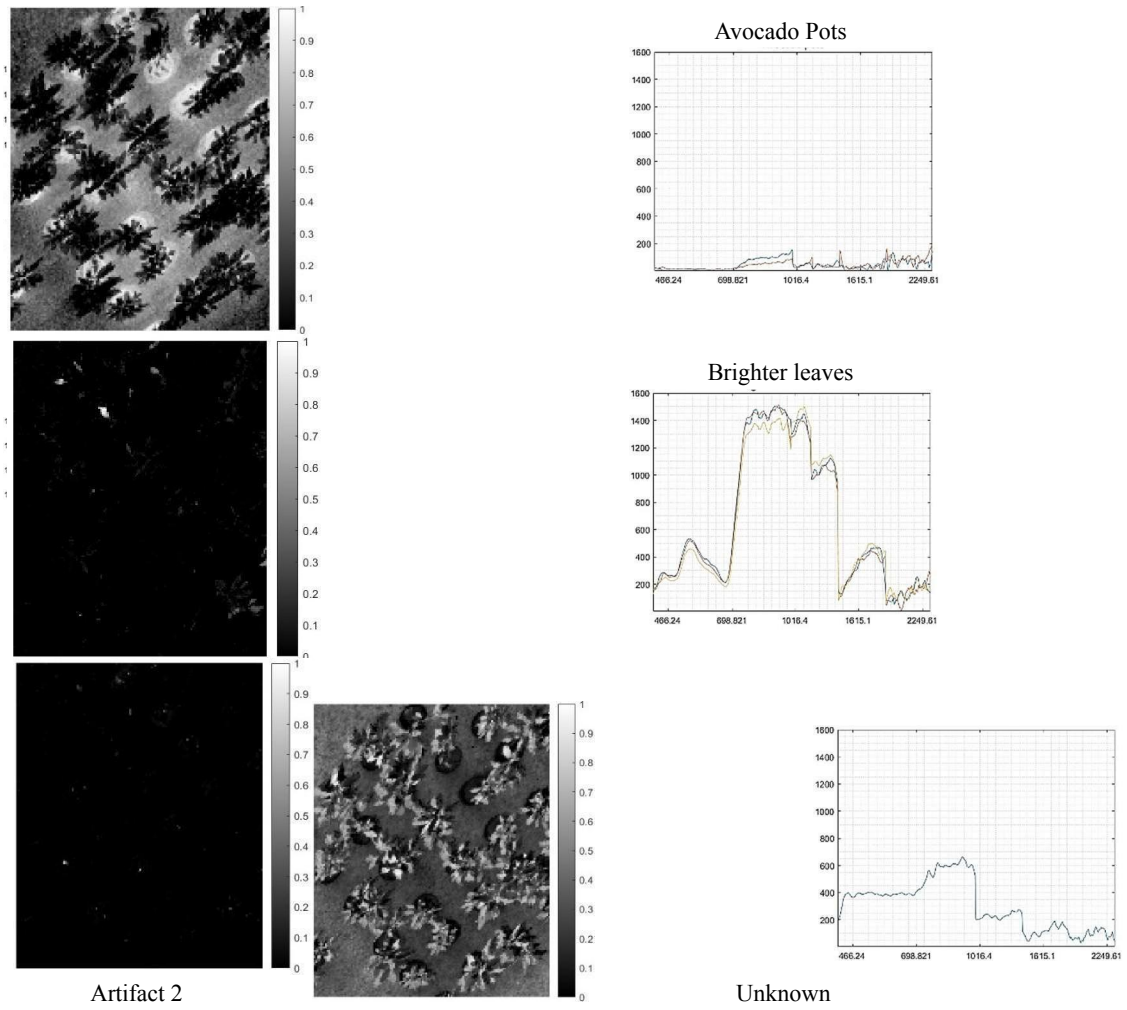

Figure 4: Endmember classes and abundances for Avocados image.

Table 2: Number of spectral endmembers per endmember class.

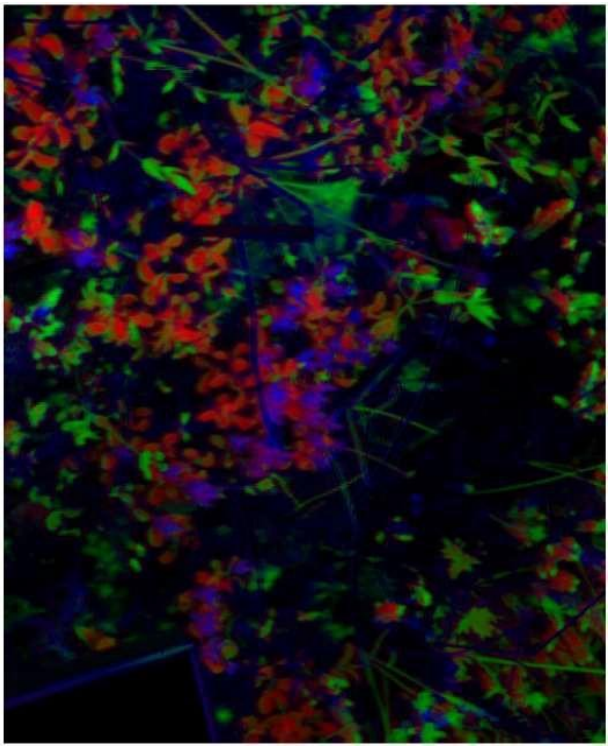

TEX Vegetation		Avocado Trail	
Signature	# of signatures	Signature	# of signatures
Shadow	7	Avocado plants	3
White standard	3	Avocado pots	2
Cassiope Tetragona	2	Avocado Artifact 1	6
Lichen Mixture 1	1	Avocado Artifact 2	5
Lichen Mixture 2	1	Brighter avocado leaves	3
Wooden Marker frame	2	Unknown	1
Wood marker	1		

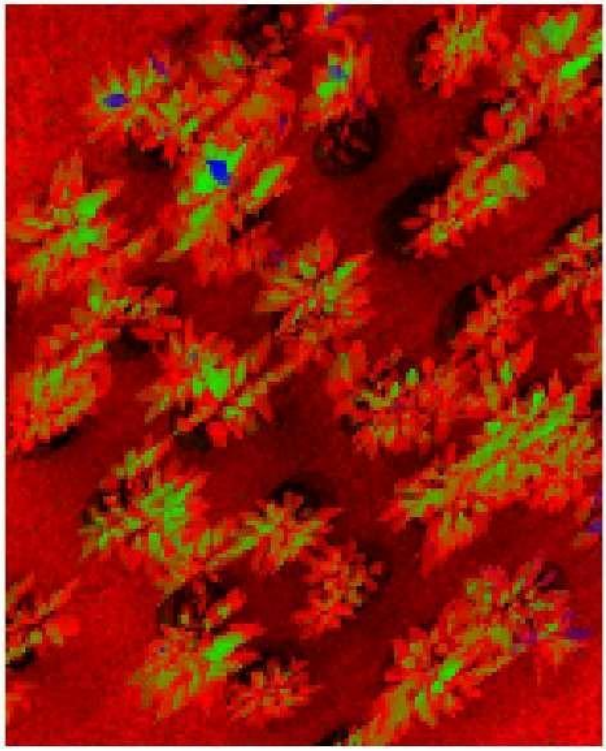

3.2 Discussion

(a)

(b)

Figure 5: Fractional Maps: (a) ITEX plot, (b) Avocados image.

Figure 3 and Figure 4 illustrate the extracted endmember classes and their corresponding abundance maps, for the two images. The approach was capable of extracting the vegetation signatures in both images.

In Figure 3, for the ITEX plot image, the endmember class with the higher number of spectral signatures was shadows with seven spectral endmembers. We were able to capture the shadow endmember because of the modification to PPI to include votes for the minimum in the projection. In experiments not included in the paper, standard PPI implementations that only count votes for the maximum do not extract the shadow endmember neither do other standard endmember extraction algorithms that we tried in for problem. Notice that the abundance map points to the significant presence of this endmember across the image, which is also shown in Figure 1(a).

An interesting finding for the Avocados image were the “Artifact” endmembers shown in Figure 4. It seems that there is a miss registration error between the two instruments in the Dual HySpex Mjolnir VS-620. For instance, the VNIR signature collected with HySpex Mjolnir V-1240 seems to be Artifact 1 while Artifact 2 seems to be the SWIR signature collected with HySpex Mjolnir S-620. One can merge the signature of Artifact 1 with 2 and get the Avocado spectral endmember signatures.

Another interesting result is that the fractional color maps are dominated by pure red, green or blue pixels. There are no pixels with color mixtures (e.g. Green + Red = Yellow) pointing to the purity of the pixels in the image as expected for VHSR-HSI.

4. CONCLUSIONS

Endmember extraction techniques offer valuable means for extracting spectral signatures of materials in a VHSR-HSI and capture their spectral variability. The abundance maps provide information on the spatial distribution of the pure materials in the image and most abundance values seem to be close to one as expected for VHSR-HSI. These abundance maps may provide simpler features for other processing stages in the HSI exploitation pipeline. The effectiveness of unmixing techniques is especially evident when analyzing intricate hyperspectral images like the one for the ITEX plot, which has significant spatial complexities due to the way materials are distributed in the image an illumination issues.

Estimating the number of endmembers using the PPI votes histogram is an interesting proposition. Clearly, we need more work to figure out systematic ways to deal with threshold selection but it address limitations of methods commonly used in the literature that use versions of a matrix rank.

These preliminary results show the potential the unmixing can have for VHSR-HSI.

5. ACKNOWLEDGMENTS

The authors would like to thank Dr. Sergio Vargas from UTEP for helping labeling the data from the ITEX vegetation plots. Support for Dr. Maria C. Torres-Madroñero and Mr. Manuel Goez-Mora is provided by the Ministerio de Ciencia, Tecnología e Innovacion—Minciencias, Colombia under grant number RC 80740-475-2020. Dr. Velez-Reyes received partial support for this work from The National Oceanic and Atmospheric Administration Educational Partnership Program
– Cooperative Science Center for Earth System Sciences and Remote Sensing Technologies (NOAA/EPP-CESSRST) under the Cooperative Agreement Grants #: NA16SEC4810008 and NA22SEC4810016. The views and conclusions contained herein are those of the authors and should not be interpreted as necessarily representing the official policies or endorsements, either expressed or implied of NOAA or the U.S. Government.

6. REFERENCES

[1] T. H. Kurz and S. J. Buckley, "A review of hyperspectral imaging in close range applications," ISPRS - International Archives of the Photogrammetry, Remote Sensing and Spatial Information Sciences, Vols. XLI-B5, p. 865–870, June 2016.

[2] P. Mishra, M. S. M. Asaari, A. Herrero-Langreo, S. Lohumi, B. Diezma and P. Scheunders, "Close range hyperspectral imaging of plants: A review," Biosystems Engineering, vol. 164, p. 49–67, December 2017.

[3] D. Krupnik and S. Khan, "Close-range, ground-based hyperspectral imaging for mining applications at various scales: Review and case studies," Earth-Science Reviews, vol. 198, p. 102952, November 2019.

[4] J. M. Bioucas-Dias, A. Plaza, N. Dobigeon, M. Parente, Q. Du, P. Gader and J. Chanussot, "Hyperspectral Unmixing Overview: Geometrical, Statistical, and Sparse Regression-Based Approaches," IEEE Journal of Selected Topics in Applied Earth Observations and Remote Sensing, vol. 5, p. 354–379, April 2012.

[5] N. Keshava, "A survey of spectral unmixing algorithms," Lincoln laboratory journal, vol. 14, p. 55–78, 2003.

[6] W.-K. Ma, J. M. Bioucas-Dias, T.-H. Chan, N. Gillis, P. Gader, A. J. Plaza, A. Ambikapathi and C.-Y. Chi, "A signal processing perspective on hyperspectral unmixing: Insights from remote sensing," IEEE Signal Processing Magazine, vol. 31, p. 67–81, 2013.

[7] J. W. Boardman, F. A. Kruse and R. O. Green, "Mapping target signatures via partial unmixing of AVIRIS data," in Summaries of the Fifth Annual JPL Airborne Earth Science Workshop, 1995.

[8] J. R. Schott, Remote Sensing: The Image Chain Approach, Oxford University Press, 2007.

[9] S. Rosario-Torres and M. Velez-Reyes, "An algorithm for fully constrained abundance estimation in hyperspectral unmixing," in Proceedings of SPIE, 2005.

[10] R. A. Schowengerdt, Remote Sensing: Models and Methods for Image Processing, 3 ed., Elsevier, 2007.